

This is a copy of the published version, or version of record, available on the publisher's website. This version does not track changes, errata, or withdrawals on the publisher's site.

Status Update on the Development of METIS, the Mid-Infrared ELT Imager and Spectrograph

Bernhard Brandl, Felix Bettonvil, Roy van Boekel, Adrian
Glauser, Sascha Quanz, et al.

Published version information:

Citation: BR Brandl et al. Status update on the development of METIS, the midinfrared ELT imager and spectrograph. Proc SPIE 12184 (2022): 1218421. Is in proceedings of: Conference on Ground-Based and Airborne Instrumentation for Astronomy IX, Montréal, Québec, Canada, 17-22 Jul 2022

DOI: [10.1117/12.2628331](https://doi.org/10.1117/12.2628331)

Copyright 2022 Society of Photo-Optical Instrumentation Engineers (SPIE). One print or electronic copy may be made for personal use only. Systematic reproduction and distribution, duplication of any material in this publication for a fee or for commercial purposes, and modification of the contents of the publication are prohibited.

This version is made available in accordance with publisher policies. Please cite only the published version using the reference above. This is the citation assigned by the publisher at the time of issuing the APV. Please check the publisher's website for any updates.

This item was retrieved from **ePubs**, the Open Access archive of the Science and Technology Facilities Council, UK. Please contact epublications@stfc.ac.uk or go to <http://epubs.stfc.ac.uk/> for further information and policies.

PROCEEDINGS OF SPIE

[SPIDigitalLibrary.org/conference-proceedings-of-spie](https://spiedigitallibrary.org/conference-proceedings-of-spie)

Status update on the development of METIS, the mid-infrared ELT imager and spectrograph

Bernhard Brandl, Felix Bettonvil, Roy van Boekel, Adrian Glauser, Sascha Quanz, et al.

Bernhard R. Brandl, Felix Bettonvil, Roy van Boekel, Adrian Glauser, Sascha P. Quanz, Olivier Absil, Markus Feldt, Paulo J. V. Garcia, Alistair Glasse, Manuel Guedel, Lucas Labadie, Michael Meyer, Eric Pantin, Shiang-Yu Wang, Hans van Winckel, Tibor Agócs, António Amorim, Thomas Bertram, Leonard Burtscher, Christian Delacroix, Werner Laun, Dirk Lesman, Gert Raskin, Chad Salo, Silvia Scheithauer, Remko Stuik, Stephen Todd, Christoph Haupt, Ralf Siebenmorgen, "Status update on the development of METIS, the mid-infrared ELT imager and spectrograph," Proc. SPIE 12184, Ground-based and Airborne Instrumentation for Astronomy IX, 1218421 (29 August 2022); doi: 10.1117/12.2628331

SPIE.

Event: SPIE Astronomical Telescopes + Instrumentation, 2022, Montréal, Québec, Canada

Status Update on the Development of METIS, the Mid-Infrared ELT Imager and Spectrograph

Bernhard R. Brandl^{*a,b}, Felix Bettonvil^{a,c}, Roy van Boekel^d, Adrian Glauser^e, Sascha P. Quanz^e, Olivier Absil^f, Markus Feldt^d, Paulo J. V. Garcia^g, Alistair Glasse^h, Manuel Guedel^j, Lucas Labadie^k, Michael Meyer^l, Eric Pantin^m, Shiang-Yu Wangⁿ, Hans van Winckel^o, Tibor Agócs^c, Antonio Amorim^g, Thomas Bertram^d, Leonard Burtscher^a, Christian Delacroix^f, Werner Laun^d, Dirk Lesman^c, Gert Raskin^o, Chad Salo^a, Silvia Scheithauer^d, Remko Stuik^{a,c}, Stephen Todd^h, Christoph Haupt^p, Ralf Siebenmorgen^p, & many more invaluable METIS Team members

^aLeiden Observatory, Leiden University, P.O. Box 9513, 2300 RA Leiden, The Netherlands;

^bFaculty of Aerospace Engineering, Delft University of Technology, Kluyverweg 1, 2629 HS Delft, The Netherlands;

^cNOVA Optical and Infrared Instrumentation Group, P.O. Box 2, 7990 AA Dwingeloo, The Netherlands;

^dMax-Planck-Institut für Astronomie, Königstuhl 17, 69117 Heidelberg, Germany;

^eSwiss Federal Institute of Technology (ETH Zürich), Department of Physics, Institute for Particle Physics and Astrophysics, Wolfgang-Pauli-Strasse 27, CH-8093 Zürich, Switzerland;

^fUniversité de Liège, STAR Institute, 19c allée du Six Août, B-4000 Liège, Belgium;

^gUniversidade do Porto, Faculdade de Engenharia, CENTRA research unit - SIM group, Rua Dr. Roberto Frias, 4200-465 Porto, Portugal

^hUK Astronomy Technology Centre, Edinburgh EH9 3HJ, UK;

^jUniversity of Vienna, Department of Astrophysics, Türkenschanzstrasse 17, A-1180 Vienna, Austria;

^kI. Physikalisches Institut, Universität zu Köln, Zùlpicher Straße 77, 50937 Köln, Germany;

^lUniversity of Michigan, Department of Astronomy, 1085 S. University, Ann Arbor, MI 48109, USA

^mCommissariat à l'Énergie Atomique, Institut de Recherche sur les Lois Fondamentales de l'Univers, Service d'Astrophysique, Orme des Merisiers, 91191 Gif sur Yvette, France;

ⁿAcademia Sinica, Institute of Astronomy and Astrophysics, Roosevelt Rd, Taipei 10617, Taiwan

^oInstituut voor Sterrenkunde, K.U.Leuven, Celestijnenlaan 200D, B-3001 Leuven, Belgium;

^pEuropean Southern Observatory, Karl-Schwarzschild-Str. 2, 85748 Garching bei München, Germany;

ABSTRACT

The Mid-Infrared ELT Imager and Spectrograph (METIS) is one of the first generation science instruments on ESO's 39m Extremely Large Telescope (ELT). METIS will provide diffraction-limited imaging and medium resolution slit-spectroscopy from 3 – 13 microns (L, M, and N bands), as well as high resolution ($R \sim 100,000$) integral field spectroscopy from 2.9 – 5.3 microns. Both imaging and IFU spectroscopy can be combined with coronagraphic techniques. After passing its preliminary design review (PDR) in May 2019, and the final design review (FDR) of its optical system in June 2021, METIS is now preparing for the FDR of its entire system in the fall of 2022, while the procurements of many optical components have already started. First light at the telescope is expected in 2028, after a comprehensive assembly integration and test phase. In this paper we focus mainly on the various design aspects, and present a status update on the final optical and mechanical design of METIS. We describe the conceptual setup of METIS, its key functional components, and the resulting observing modes. Last but not least, we present the expected scientific performance, in terms of sensitivity, adaptive optics, and high contrast imaging performance.

Keywords: METIS, ELT, mid-infrared, infrared spectroscopy, high-contrast imaging, exoplanets, proto-planetary disks, calibration

1. PROJECT OVERVIEW

1.1 Context

The Mid-Infrared ELT Imager and Spectrograph (METIS) will be one of four first-generation instruments on ESO's Extremely Large Telescope (ELT). METIS will work on the Nasmyth platform of the ELT alongside the High Angular Resolution Monolithic Optical and Near-infrared Integral field spectrograph (HARMONI), the Multi-Adaptive Optics Imaging Camera for Deep Observations (MICADO), and MORFEO (Multiconjugate adaptive Optics Relay For ELT Observations).

With its coverage of the thermal infrared wavelength range (3 – 13 μm), METIS fills a unique and scientifically important niche, not only at the ELT but among the first generation of instruments on extremely large telescopes in general. A general, brief overview can be found in the ESO Messenger [1].

METIS is being designed and built by a consortium of 12 partner institutes from 10 countries (8 European, 1 US, 1 Taiwan), in close partnership with ESO. The Consortium partners are: NOVA (NL, project office U Leiden), MPIA (DE), UK-ATC (UK), CEA Saclay (FR), ETH Zürich (CH), A* (AT), ASIAA (TW), Centra (PT), U Cologne (DE), KU Leuven (BE), U Liège (BE), and U Michigan (US). The status of METIS has been reported in several previous SPIE proceedings [2], [3], [4], [5].

1.2 Instrument Baseline

The first images from the JWST impressively demonstrated the unsurpassed sensitivity in the infrared that can only be achieved with a cooled telescope from space. However, ground-based infrared facilities have several unique advantages, most notably that the telescope aperture can be much bigger (enabling six times higher angular resolution (ELT/JWST), the instruments can be bigger (allowing for large high resolution spectrographs), and the instruments can be serviced and upgraded with the most recent technology.

The instrument baseline of METIS has been determined with these considerations in mind. METIS will offer a combination of high angular resolution, high contrast imaging (HCI) by means of coronagraphy, and high spectral resolution (up to $R \sim 100,000$). The two fundamental observing functionalities of METIS will be:

1. Direct imaging at 3 – 13 μm , including:
 - medium resolution ($R \sim 1400 @ L/M$; $R \sim 400 @ N$) long-slit spectroscopy
 - coronagraphy for high contrast imaging
2. High resolution ($R \sim 100,000$) integral-field spectroscopy at 3 – 5 μm , including:
 - a mode with extended instantaneous wavelength coverage $\Delta\lambda_{\text{instant}} \sim 300 \text{ nm}$
 - coronagraphy for high contrast IFU spectroscopy

The fields of view (FoV) of these modes are depicted in Figure 1. In all its modes and at all wavelengths, METIS will operate with adaptive optics (AO) to correct for atmospheric turbulence and to achieve the best possible point-source sensitivity at the diffraction limit of the 39m ELT ($\sim 23 \text{ mas} @ 3.5\mu\text{m}$). METIS will generally operate in the Background Limited Performance (BLIP) regime.

1.3 Science Drivers

METIS will be a versatile instrument, targeting a wide range of science applications in a cool and dusty Universe. These include investigations of Solar System objects, young stellar clusters and massive star formation, active galactic nuclei (AGN), evolved stars, the centre of our Milky Way, and star formation in other galaxies. Its main science drivers, however, are the studies of exoplanets and proto-planetary disks [1].

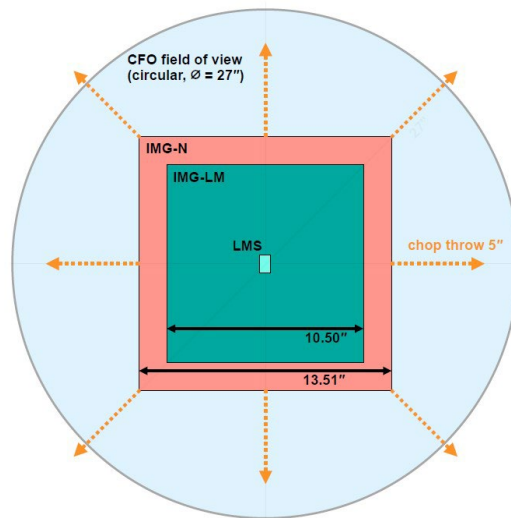


Figure 1 The fields of view in METIS. The larger FoV of the common fore-optics (indicated in light blue) allows chopper offsets of up to 5" in all directions as well as AO guide star pick-up within this field. The FoV of the LM- and N-band arms of the imager are shown in green and red, respectively. The FoV of the integral-field spectrograph is $0.''58 \times 0.''93$, shown here in the center (LMS).

METIS will provide access to those regions of protoplanetary disks, where the bulk of terrestrial planet formation takes place, and will extend the current ALMA studies of disk kinematics and (molecular) composition toward the inner regions of the disk. A key aspect will be the distribution of water and organics in the innermost disk regions (e.g., [6], [7]) and the use of isotopologue abundances (e.g., of CO) to investigate the mixing of material within a large number of disks (e.g., [8], [9]). Identifying signatures of ongoing planet formation and even the direct detection of young forming planets embedded within disks from kinematical imprints (see, e.g., [10], [11] for studies using ALMA) is another showcase of METIS' capabilities. It is these applications that drive the requirements for the high-dispersion IFU mode in the L and M band. For the first time, disk gaps and sub-structures, frequently detected with ALMA at (sub-)mm wavelengths (e.g., [12]) and with SPHERE on ESO's VLT at near-infrared wavelengths in scattered light (e.g., [13]), can be revealed with comparable spatial resolution in the MIR.

Truly new science is expected from the direct detection of extrasolar planets, e.g. by constraining the luminosities of gas giant exoplanets that have an empirical mass estimate from radial velocity measurements (or soon from astrometry with GAIA). The high-dispersion IFU mode in the L and M band will allow the exoplanet community to expand significantly upon the work pioneered with CRILES (and soon CRILES+) to detect and characterize the atmospheric composition and dynamics of hot – and with METIS also warm – exoplanets (e.g., [14], [15]). In addition, METIS will be able to investigate less massive, Saturn- and Neptune-like objects, and not only the Jupiter-class objects accessible today. Finally, it is expected that METIS will take the first steps towards the direct detection and characterization of nearby temperate terrestrial exoplanets. Following up on the NEAR experiment [16] on the VLT, METIS will be able to observationally test whether our nearest neighbours harbour rocky worlds (cf. [17]). For the very nearest star, Proxima Centauri, that is known to host a rocky, temperate planet [18], METIS will be able to directly detect the planet and – possibly – probe its atmospheric composition.

1.4 Observing Modes and Instrument Configurations

METIS offers five main observing modes, which are listed in Table 1. These observing modes can be used in 19 different instrument configurations, not accounting for different science and neutral density filters. Each of these configurations is driven by one or more specific science observation(s), which are also listed in Table 1. Not explicitly shown in Table 1 are the two additional parallel modes: (i) simultaneous direct imaging at L/M-band and at N-band; (ii) simultaneous longslit spectroscopy of compact sources at L/M-band and at N-band. It is noteworthy that high resolution

IFU spectroscopy is, by default, done in combination with direct imaging at L/M-band to have a relative astrometric reference frame.

Table 1 The five main observing modes of METIS and their resulting 19 instrument configurations (excluding parallel modes), together with their main science drivers.

Science Observing Mode	Instrument Configuration						Science Driver
	Sub-Syst.	Band	IFS Setting	HCI Mask	P T	F T	
Direct Imaging	IMG	L,M	N/A	N/A	•	•	circum-stellar (YSOs) and circum-nuclear (AGN) structures, star clusters
	IMG	N	N/A	N/A	•	•	circum-stellar (YSOs) and circum-nuclear (AGN) structures
High Contrast Imaging	IMG	L,M	N/A	RAVC/CVC	•	•	exoplanets (detection + characterization)
			N/A	APP	•	•	
	IMG	N	N/A	CVC	•	•	exoplanets (detection + characterization)
Longslit spectroscopy	IMG	L,M	N/A	N/A	•	•	ices in comets and star forming regions
	IMG	N	N/A	N/A	•	•	physics of circum-stellar and circum-nuclear environments; solid-state chemistry & mineralogy
IFU spectroscopy	LMS	L,M	full IFU field	N/A	•	•	kinematics and chemistry of circum-stellar environments
	LMS	L,M	spectral IFU $\Delta\lambda\sim 300\text{nm}$	N/A	•	•	chemical studies of the interstellar medium
IFU+HCI spectroscopy	LMS	L,M	full IFU field	APP	•	•	exoplanetary atmospheres at $\theta > 3\lambda/D$, pp-disks
				RAVC/CVC	•	•	exoplanetary atmospheres at $\theta \sim 2\lambda/D$, pp-disks
	LMS	L,M	spectral IFU $\Delta\lambda\sim 300\text{nm}$	APP	•	•	exoplanetary atmospheres at $\theta > 3\lambda/D$
				RAVC/CVC	•	•	exoplanetary atmospheres at $\theta \sim 2\lambda/D$

Because METIS is located at the telescope Nasmyth focus, it is equipped with an (internal, cryogenic) de-rotator that needs to be rotated to preserve the orientation of either the telescope pupil or the focal plane for the duration of an observation. It is referred to either pupil tracking (PT) or field tracking (FT) in Table 1.

The telescope support structure (spiders) provides a bright and spatially inhomogeneous contribution to the background emission, which should be masked out to minimize the thermal background emission from the telescope. METIS is equipped with the corresponding cryogenic pupil plane masks in the imager and LM-band IFU spectrograph. However, these masks have a fixed orientation, and are therefore not optimal for field-stabilized observations, where the projected telescope pupil rotates within the instrument. For this reason, we foresee METIS observations to be performed in pupil tracking mode whenever possible, with the image derotation performed in post-processing. Observations that require field-tracking will be performed without spider masks, and will suffer from a somewhat higher thermal background.

1.5 Project Schedule

At the point in time of this proceedings paper, the METIS project is in full swing, preparing for the final design review (FDR) of the entire system in November 2022. The main project milestones are shown in Table 2. The FDR has been split to allow for the timely start of the procurement of long-lead items (mostly the ICAR cryogenic motors – see Figure 4, optics components, and detectors).

Table 2 The main project milestones.

Milestone	Focus	Date	Comment
Phase-B kick-off		Nov 2015	done
Preliminary design review (PDR)		May 2019	passed
Final design review (FDR)	Motorized mechanisms (ICARs)	March 2021	passed
	Optical system	May 2021	passed
	System FDR (rest)	November 2022	in prep.
System MAIT		Mid 2024 - 2027	
Preliminary Acceptance Europe (PAE)		Early 2028	
Commissioning @ELT		2028	

2. DESIGN CONCEPT

2.1 Design Overview

METIS consists of two science modules: (1) A diffraction-limited imager with two wavelength channels, one for the LM-band and one for the N-band, and (2) an Integral Field Unit (IFU)-fed, diffraction-limited, high-resolution LM-band spectrograph. Both of these science modules are served by the common fore-optics (CFO). Figure 2 illustrates the conceptual setup of METIS: The light from the ELT enters through the entrance window into the CFO, which conditions the beam from the telescope in various ways (see section 2.2 for details). Here the beam is spectrally split between the AO wavefront sensor (WFS) module (1.4 – 2.4 μm) and the science beam (3 – 13 μm). At the end of the CFO, the full science beam gets either passed on to the imager (IMG) or its central part gets reflected into the high resolution IFU spectrograph (LMS).

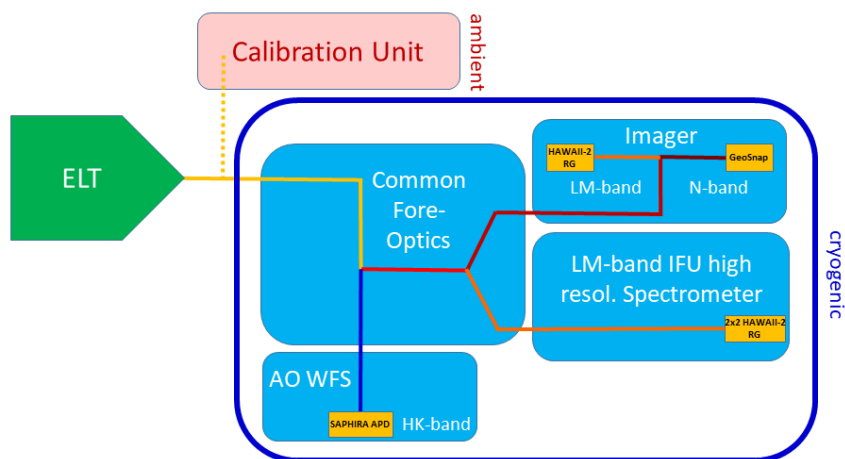


Figure 2 Simplified block diagram illustrating the conceptual setup of METIS. The colors of the beam qualitatively refer to the transmitted infrared wavelengths.

All optics are cryogenically cooled to ~ 70 K with the exception of the imager at ~ 40 K and the science detectors at 30-40 K. (The SAPHIRA WFS detector will be operated at ~ 100 K). A cryostat provides the cryo-vacuum environment using three 2-stage PT810 pulse-tube coolers and liquid nitrogen for its radiation shields. The cooldown of the entire instrument will take about one week and require ~ 5000 liters of LN_2 for precooling.

The cryostat is supported by a support structure, which also lifts the instrument to the 6 m height of the optical axis of the ELT beam above the Nasmyth platform. On top of the cryostat sits the warm calibration unit (WCU) which provides important test and calibration means during MAIT [35] and daytime operations.

2.2 Design Explanation

Figure 3 shows the functional diagram of the METIS optical system, including all functional optical components. Also shown are the intermediate pupil and focal planes within the cold optics. The relatively large number of reimaged pupils is required by the needs of background/straylight reduction, coronagraphy, and spectroscopy for dedicated pupil and focal plane masks in a specific order. Here we describe the various subsystems, in the order of the beam propagation (Figure 3) in more detail. For a more “practical experience” the reader is referred to the METIS-App at <https://metis-app.strw.leidenuniv.nl/>, which allows the user to configure the instrument in various ways and set up an observation.

Common Fore Optics (CFO)

The CFO is the core optical subsystem of the instrument, which reimages the central 27" of the ELT focal plane, and supports the instrument subsystems by providing essential functionalities. The most significant ones are briefly described below.

The optical system of the CFO consists mainly of spherical mirrors, which are milled from aluminium RSA-6061 and post-polished by the NOVA Optical and Infrared Instrumentation Group [19], [20].

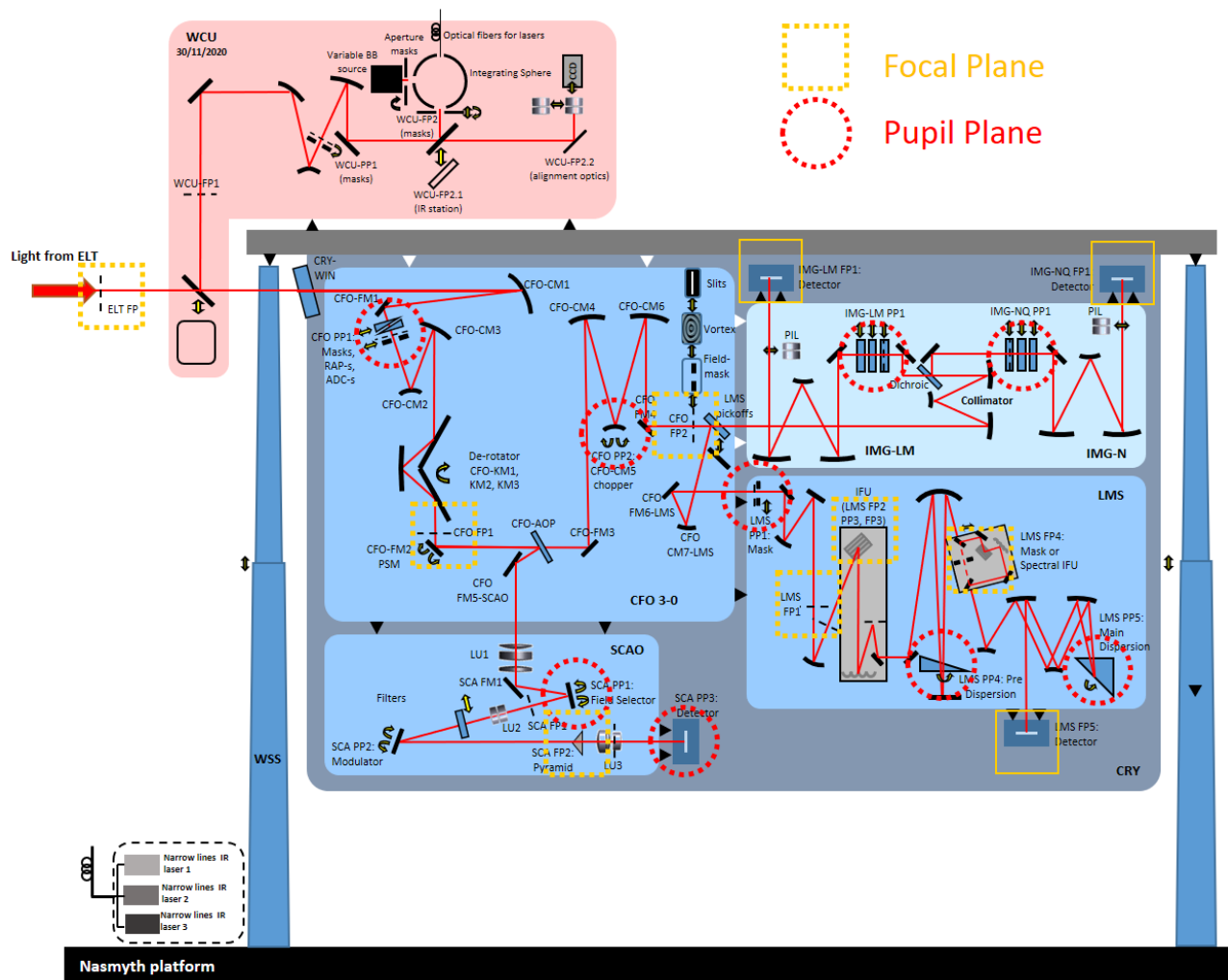


Figure 3 Functional diagram of the optical system within METIS, with a layout similar to Figure 2. All functional optical components are represented here; the beam is reduced to the optical axis. The main intermediate focal and pupil planes are indicated by yellow squares and red circles, respectively. (We note that both the LMS and the SCAO subsystem possess additional pupil and focal planes, which are not indicated here for better visibility).

Atmospheric differential dispersion causes the monochromatic images of a celestial source to be spatially offset with respect to other wavelengths in the direction perpendicular to the horizon. In broad-band observations, this causes a smearing of the PSF. In order to compensate for this effect, two pairs of rotating prisms – to optimally compensate the effect for all zenith angles – are often used. However, a retractable, rotating double prism assembly would be very complex to realize in the cryogenic environment of METIS. Therefore, we have implemented a simplified solution, based on two sets of “fixed Atmospheric Dispersion Compensation (ADC)” prisms in the first pupil plane (PP1), one optimized for a zenith angle of 25 deg, and one optimized for 41 deg. For observations close to zenith, METIS will operate without ADC, for zenith angles between ~ 15 deg and ~ 35 deg the first fixed ADC will be used, and for zenith angles larger than ~ 35 deg, the second fixed ADC will be utilized. Although the correction achieved in this way will not be perfect, the partial correction still results in a much better PSF, that enables very efficient coronagraphy.

Following the pupil plane PP1 is the **derotator**, which is located just before the first focal plane (FP1) and positioned in a gravity invariant (vertical) orientation. The derotator (often referred to as “K-mirror” due to its composition of three flat mirrors) rotates slowly in order to stabilize either the field or the pupil orientation within METIS.

FP1 marks location of the **pupil stabilization mirror** which ensures the tight co-alignment of the various pupils between METIS and the ELT. Potential displacements due to the telescope and/or the derotator are measured by the METIS AO

wavefront sensor, and corrected in closed-loop. After FP1, the light is spectrally split by a dichroic, which directs the near IR light (H & K bands) into the Single Conjugated Adaptive Optics (SCAO) subsystem to feed the cryogenic AO wavefront sensor.

Traditionally, chopping – a method to measure and subtract the thermal background – is performed with the telescope’s secondary mirror, often leading to significant chop residuals that are removed with additional nodding (i.e. corresponding repointings of the telescope). With the ELT, however, this classical chopping scheme cannot be performed, and we have developed a fast, cryogenic, 2-D **beam chopper** (Figure 4) [21] which allows us to switch between the target and a nearby reference sky. To our best knowledge, this is a first in ground-based thermal infrared astronomy at large telescopes. Chopping inside the instrument, behind the entrance window and six warm mirrors upstream of METIS, is expected to lead to substantial chopping residuals. A large effort is therefore being undertaken to better understand the residuals after thermal background removal in current instruments and to transfer this knowledge to ELT/METIS, including the testing of new background subtraction techniques on the way to achieve photon shot-noise limited performance. The chopper mechanism will also be essential during system Assembly, Integration, and Test (AIT) and regular operations in order to steer calibration point sources across the field. The cryogenic beam chopper is located at the second pupil location of the CFO (PP2).

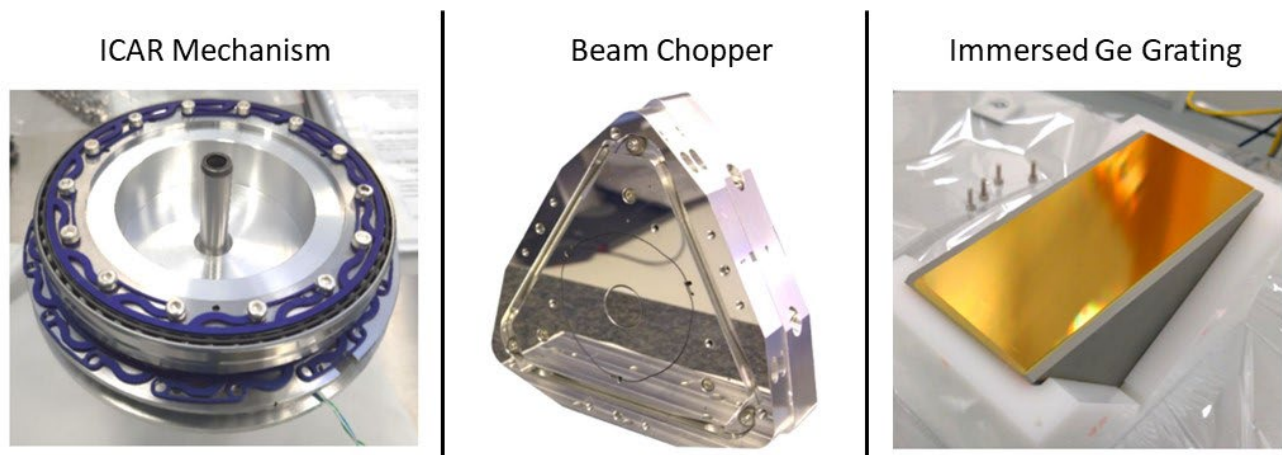


Figure 4 Some representative hardware items that have already been procured for METIS: Left: the Indexed Cryogenic Actuator for Rotation (ICAR) motors that drive many of the METIS mechanisms with high accuracy and reliability; Center: the fast (< 5 msec), precise (~ 1 marsec stability) cryogenic beam chopper which allows up to $\pm 5''$ offsets, a joint development with Janssen Precision Engineering (JPE in the Netherlands) [21]. Right: the Germanium-based high-resolution, immersed grating with an 18.2 μm pitch and a grating flatness of 7.5 nm at Littrow condition. The grating was made by Canon, Japan [25].

The subsequent, second focal plane of the CFO (FP2) contains two focal plane wheels with numerous field stops, slits, coronagraphic masks, alignment masks and a retractable beam splitter which (if engaged) directs light into the LMS, or passes it on to the IMG subsystems.

Single Conjugate AO System

The SCAO subsystem of METIS enables observations at or near the diffraction limit. It uses the light of a single near-infrared, natural “guide star” to measure the phase of the incoming wavefront. The use of a laser guide star system, while scientifically desirable, is not part of the current METIS baseline for financial reasons. The wavefront correction is applied in real-time by controlling the adaptive mirrors of the ELT [22]. The three main components of the AO system hence are:

1. A Pyramid-type wavefront sensor inside the METIS instrument, working at near-infrared (H, K-bands) wavelengths. The WFS is equipped with opto-mechanical actuators for field selection within the 27" wide FoV (although in most cases the science target itself will be used as “guide star”), and modulation of the “guide star”. The WFS runs at a maximum loop frequency of 1 kHz (optimized for contrast).

2. A fast, “Real-Time” Computer (RTC), which computes the necessary corrections to be applied to the wavefront.
3. A deformable mirror and a tip-tilt mirror that apply these corrections to the incoming wavefront. These mirrors, M4 and M5, are integral parts of the ELT. With over 5000 actuators, these correcting elements will approximate “extreme” AO correction at the infrared wavelengths of METIS (section 4.2)

Imager

The imager covers the wavelength range from L to N band (approximately 3 – 13 μm). For optimal performance, this wavelength range is split into two channels, which are equipped with two different science detectors [23]. The imager has a collimator, that is common to both channels, and two camera optics optimized for the field of view (Figure 1), defined by the science detectors and the required sampling (5.5 marcsec pixels at L/M band and 6.8 marcsec pixels at N-band). The light is split in wavelength by a dichroic in the collimated beam, followed by a set of filters, pupil masks and grisms at the pupil position that can be inserted into the beams. A Three-Mirror-Anastigmat (one TMA per channel) focuses the light onto the science detector. The two channels of the imager can be operated in parallel, in either imaging or long-slit spectroscopy modes. Observations are usually performed in pupil-tracking mode for optimal background rejection, with image de-rotation and stacking of the short exposures in post-processing.

The imager subsystem also offers high contrast imaging and low-resolution spectroscopy. Both arms of the METIS imager are equipped with grisms. The long slits (which are actually located at FP2 in the CFO) offer widths from 19 – 114 marcsec; their spectral resolution is listed in Table 3. For maximum efficiency, chopping and nodding is usually done in two or more positions along the slit. Longslit observations will be performed in field-tracking mode to maintain the position angle of the slit on the sky.

The focal plane of the short-wavelength arm of the IMG will be covered with one Teledyne Imaging Systems (TIS) HAWAII-2RG (2048 \times 2048 pixel) detector, with the HgCdTe mixture tuned to provide good responsivity up to 5.3 μm . The long-wavelength arm of the IMG will be equipped with a novel 2048 \times 2048 pixel “GeoSnap” detector, also manufactured by TIS.

Coronagraphy

Coronagraphy is not a subsystem per se but deeply integrated in the CFO, IMG and LMS. We discuss it here separately due to its central importance. METIS will have two main coronagraphic concepts [24]:

- Located in the focal plane, the Classical / Ring-Apodized Vortex Coronagraphic (CVC / RAVC) mask provides starlight rejection at the smallest possible inner working angle (IWA) of around $1 \lambda/D$. It works 360° around the star and has an outer working angle (OWA) which is defined by the size of the clear aperture of the mount. Under good conditions, the RAVC provides the best performance in the speckle-dominated regime. It is however associated with a relatively low throughput, and will thus mostly be used on bright targets. The CVC provides the highest throughput of all coronagraphic modes, and will therefore be the HCI observing mode of choice to explore fainter targets. Both CVC and RAVC coronagraphs are very sensitive to pointing jitter, offsets, or drifts. Accurate positioning of the star on the CVC/RAVC will be achieved by applying the QACITS algorithm on the science data at a closed loop control frequency of ≈ 0.1 Hz.
- Located in the pupil plane, the Apodizing Phase Plate (APP) coronagraphic mask creates two conjugated, deep dark holes around two images of the central source. It provides a small IWA (around $3 \lambda/D$), a limited OWA (around $20 \lambda/D$), and – by combining both images – close to 360° discovery space for a source anywhere within the FoV. The APP is largely insensitive to pointing jitter and is therefore expected to be more robust in terms of performance for sub-optimal atmospheric conditions and/or in presence of telescope vibrations.

Table 1 shows which coronagraphic mask can be used in which observing mode. The location of most of the coronagraphic masks within METIS is schematically shown in Figure 4.

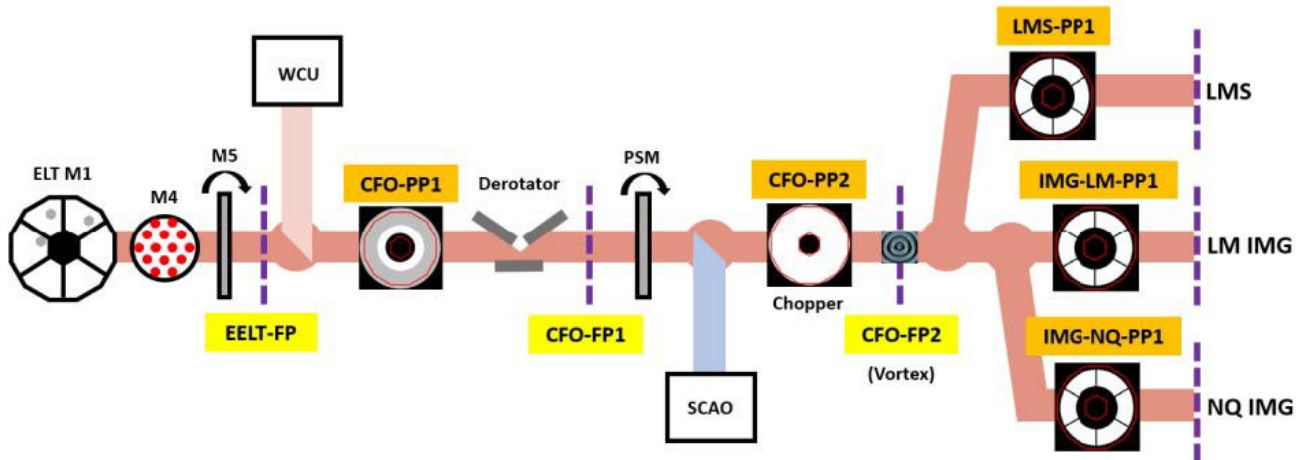


Figure 5 Schematic representation of the location of the various pupil plane (PP) and focal plane (FP) coronagraphic masks within METIS [24].

High resolution IFU Spectrograph

The high-resolution ($R \approx 100,000$) spectrograph provides integral-field spectroscopy at L and M bands. The integral field unit (IFU) optically rearranges the FoV in 28 slices, each $0.''021$ wide and $0.''93$ long, by means of a mirror slicer, followed by the pre-dispersion prism. The main dispersion is achieved by an immersed Germanium echelle grating (Figure 4) [25] in the pupil plane. The optical system uses a Three Mirror Anastigmat (TMA) in double-pass configuration. Both grism and grating are mounted on high precision rotation mechanisms to allow the selection of any wavelength in the L/M-bands.

The relatively short, nominal instantaneous wavelength coverage (Table 3) can be increased in the so-called “extended wavelength coverage” mode, in which only three slices are projected onto the focal plane, but with a larger $\Delta\lambda$ than in the nominal mode. In this way, an instantaneous wavelength coverage of up to 300 nm can be achieved at the expense of spatial coverage. The LM high resolution spectrograph can be used in combination with coronagraphy (Table 1) [36].

The focal plane of the LMS will be equipped with a 2×2 array of HAWAII-2RG (TIS) detectors with good responsivity up to $5.3 \mu\text{m}$. (Each of the four LMS detectors is identical to the IMG-LM detector).

Instrument Control System

Almost all of the METIS hardware devices will be controlled by Beckhoff Programmable Logic Controllers (PLC) through a Control Unit (CU). Among the devices that the instrument control system has to synchronize and control are:

- Ambient devices: 9 Stepper/DC motors, 6 Servo motors, 17 Vacuum gauges, 5 Vacuum pumps, 36 Valves, 3 He compressors, 3 Laser systems, 1 Black body, 1 Technical CCD, 64 Pt-100 T-sensors, and 8 T-control loops.
- Cryogenic devices: 15 Stepper mechanisms, 1 Servo motor (derotator), 1 beam chopper, 6 (Tip/Tilt) mirrors (piezo), 3 Inductosyn encoders, 9 LED illumination circuits, 125 Si-diode T-sensors, 38 Heater T-control loops, 1 Hawaii-2RG detector, 1 GeoSnap detector, 1 2×2 Hawaii-2RG detector array, and 1 Saphira (WFS) detector.

Cryostat and Support Structure

The METIS cryostat provides the cooling power for the cold structure with a mass exceeding three tons [26]. It provides the electrical feedthroughs, holds the optical entrance window, and provides the interface to the CFO. The cryostat itself is mechanically supported by a warm support structure, which provides the mechanical interface to the Nasmyth platform [27], [28], [29]. The interior of the cryostat will be cooled by three pulse tube coolers during steady state.

The cryostat vessel is divided horizontally in 3 segments. The top segment is the part where most of the cold-warm connections are made. The top flange also hosts most of the cable feedthroughs. The entrance window for the incoming light beam is also in the top segment.

Warm Calibration Unit

The warm calibration unit (WCU) subsystem is located on top of the cryostat, operates at the ambient temperature, and provides the technical functionalities to support the instrument monitoring, troubleshooting and calibration tasks [30], [31]. The WCU will be crucial to verify the internal alignment of the various METIS subsystems. More specifically, the WCU provides a set of point sources with a high enough Strehl ratio to perform the necessary alignment and calibration tasks such as image quality, distortion, plate-scale and internal wavefront sensor offsets, as well as sources for the wavelength calibration that allow for an accuracy of better than $1/5^{\text{th}}$ of a resolution element of the LMS. The WCU also provides extended broadband sources to measure the detector linearity. It also provides an ELT-like beam by means of its F-number, exit pupil location and pupil shape (the latter excluding the gaps between the mirror segments).

3. DETAILED DESIGN

3.1 Cold Optical Systems

In order to minimize mass, volume, and thermal gradients, a modular approach was used for the mechanical layout of METIS. In this concept, the cold central structure and the common fore-optics form the “heart of the instrument”. The LMS, IMG, and SCA are mounted to the sides and bottom of the cold central structure (Figure 6). The cold central structure provides the mechanical and thermal interfaces to all cryogenically cooled sub-systems, as well as the thermal interface to the pulse tube coolers for the steady state cooling. The cold central structure is also equipped with the LN₂ pre-cooling system and cold cable harnesses.

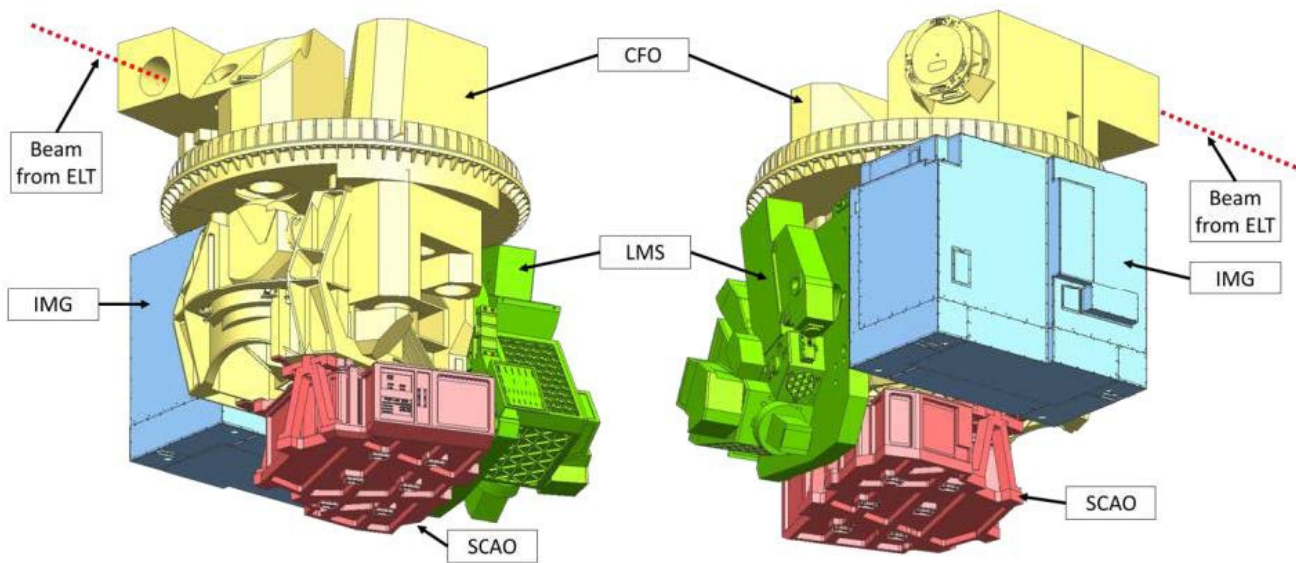


Figure 6 Two views of the mechanical design of the METIS cold optical system: the central part is the cold central structure and the common fore-optics (CFO) to which the imager (IMG) and the IFU spectrometer (LMS) are mounted. The single-conjugate adaptive optics (SCAO) wavefront sensor module is mounted at the bottom. The beam from the ELT enters horizontally near the top.

3.2 Subsystem Design Examples

Figure 7 provides an overview of the mechanical design of the the main subsystems of METIS. The representations of the common fore-optics, the LM-band IFU spectrograph, and the SCAO wavefront sensor module have been labeled and should be self-explaining. The compact imager is based on two very similar (but not identical) TMAs for the two LM- and N-band channels. The cryostat drawing clearly reveals the three segments of the cryostat vessel and illustrates the complexity required by the various electrical, mechanical, and thermal feedthroughs. Last but not least, the warm support structure (with the warm calibration unit on top) also shows the surrounding staircase, and indicates the arrangement of the electronic racks on the Nasmyth platform.

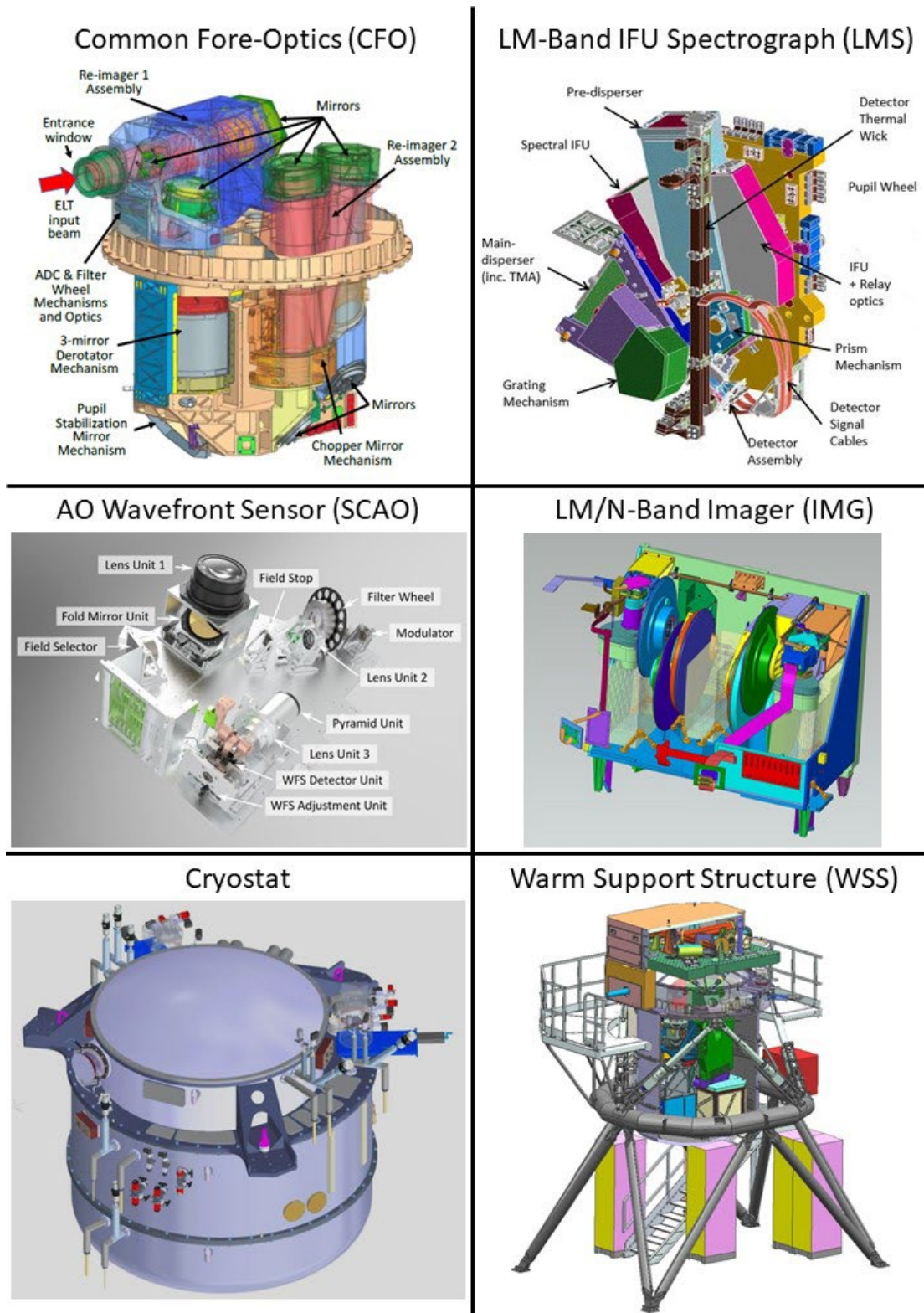


Figure 7 Opto-mechanical designs of the main subsystems of METIS (top left to bottom right): the common fore-optics, the LM-band IFU spectrograph, the SCAO wavefront sensor module, the imager, the cryostat, and the warm support structure with the warm calibration unit on top.

4. INSTRUMENT PERFORMANCE

4.1 Instrument Filters, Sensitivities, and Saturation Limits

In simple terms, thanks to the ELT's huge 39 m aperture and the high spectral resolution of the LMS, METIS will have a point source sensitivity to spectrally unresolved emission lines which is similar to that of the JWST, and a point source imaging sensitivity that is similar to that of Spitzer-IRAC. The detailed 10- σ , 1 hour sensitivities in the various observing modes and filter bands are listed in Table 3.

Table 3 The various METIS filter bands and the expected 10- σ , 1 hour sensitivities in units of Janskies. We note that the quoted sensitivities of 0.96 μ Jy correspond to $L' = 21.0$ mag, 7.6 μ Jy correspond to $M' = 18.3$ mag, and 60 μ Jy correspond to $N2 = 14.6$ mag (in the UKIRT photometric system).

	Filter	λ_c	$\Delta\lambda$	Point source	Surface brightness
Units		[μ m]	[μ m]	[μ Jy] (10- σ in 1hr)	[mJy/arcsec ²] (10- σ in 1hr)
Continuum imaging	L'	3.79	0.63	0.96	2.0
	short-L	3.31	0.43	0.72	2.0
	HCI-L short	3.60	0.22	1.06	2.4
	HCI-L long	3.82	0.27	1.46	3.0
	M'	4.80	0.60	7.6	10.0
	N1	8.65	1.16	50	20
	N2	11.20	2.36	60	14.4
Spectral feature imaging	H2O-ice	3.10	0.22	0.70	2.2
	PAH 3.3	3.30	0.07	2.6	7.0
	Br alpha	4.05	0.03	8.8	16.0
	CO(1-0)/ice	4.66	0.22	8.8	12.2
	PAH 8.6	8.60	0.45	78	32
	PAH 11.25	11.20	0.35	150	36
	[S IV]	12.82	0.23	178	48
[Ne II]	10.50	0.19	340	62	
Longslit spectroscopy	L ($R \approx 1400$)	3.53	1.3	$(2 - 6) \times 10^{-18}$ erg/s/cm ²	
	M ($R \approx 1900$)	4.9	0.8	2×10^{-17} erg/s/cm ²	
	N ($R \approx 400$)	10.50	6.0	2×10^{-16} erg/s/cm ²	
IFU spectroscopy	L ($R \approx 100k$)	3.8	0.04, 0.3	$(4 - 10) \times 10^{-19}$ erg/s/cm ²	
	M ($R \approx 100k$)	4.8	0.06, 0.3	3×10^{-18} erg/s/cm ²	

The telluric calibration is foreseen to rely primarily on fitting the observations to synthetic transmission spectra using Molecfit for a given atmospheric water vapor and temperature profile, measured by an on-site radiometer in the direction of observation.

The saturation limits for observations in the nominal imaging modes (for some representative filters) and the spectroscopic modes are given in Table 4. METIS also offers a set of neutral density (ND) filters which can be used for observing very bright targets. With these ND filters, the saturation limits for observations with the IMG-LM are increased to up to 12.5 mag brighter than the limits in Table 4, in steps of 2.5 mag. In the IMG-N arm the limits are increased with up to 10 mag in steps of 2.5 mag, in the LMS with up to 7 mag in steps of 3.5 mag.

4.2 Adaptive Optics Performance

METIS achieves fine guiding accuracies below 0.02 λ/D RMS on sky, which corresponds to 0.4 marcsec RMS at L band, and 1 marcsec RMS at N band. For bright ($K \lesssim 10$ mag, loop speed 1 kHz) AO guide stars under median/poor seeing conditions and a moderate zenith angle of 30°, METIS will achieve a Strehl ratio of $\geq 87\%$ at 3.7 μ m ($\geq 95\%$ at 10 μ m) – see Figure 8. For fainter guide stars ($K \sim 12$ mag, reduced loop of 200 Hz) this will drop to 62% at 3.7 μ m (93% at 10 μ m). These numbers assume correction for non-common path aberrations and do not include a possible performance degradation at N-band due to water vapor seeing [32] in high PWV conditions.

Table 4 Saturation limits for observations without Neutral Density (ND) filters in representative filters. Observations with the fastest full-frame DIT are assumed in all cases. For the longslit-L/M modes, the limiting magnitudes in slow/fast readout mode are given, for the longslit-N mode those for the GeoSnap low/high capacity mode.

Filter / Mode	Saturation Limit	
	[Jy]	[mag]
L'	0.049	9.2
Br α	2.2	4.9
HCl-L long	0.14	8.1
CO (1-0)/ice	0.35	6.7
N ₂	7.2	1.6
PAH 8.6	9.3	1.9
[Ne II]	83	-1.4
Longslit L		6.0 / 2.5
Longslit M		3.6 / 0.1
Longslit N		-0.4 / -3.2
LMS-L		3.0
LMS-M		1.1

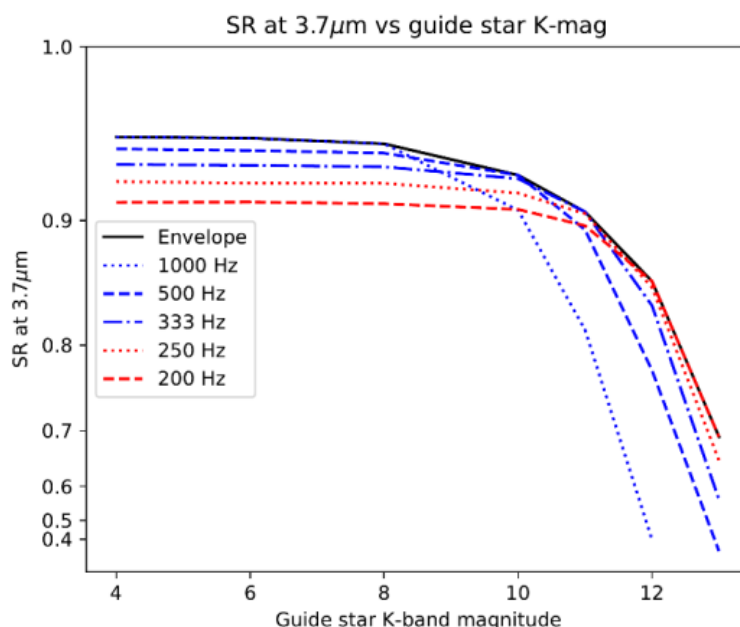


Figure 8 Performance of the METIS AO system, expressed in terms of the Strehl ratio at 3.7 μm for a range of guide star magnitudes at K-band. For bright sources, the performance exceeds the classical diffraction limit (80% SR) by a significant margin. For fainter sources, the performance can be improved by reducing the speed of the WFS readout and thus the AO control loop [22].

4.3 High Contrast Imaging Performance

The excellent optical performance of the METIS AO system (section 4.2) enables efficient coronagraphy and high contrast imaging [33], [34]. Since the theoretical contrast curves are generally quite optimistic for the real environment at the telescope, we have included several likely perturbations in our simulations, such as pupil drift, Talbot effect, residual non common path aberrations (NCPA) and the effect of a cluster of 7 slightly misaligned ELT M1 segments. As can be seen in Figure 9 these effects reduce the achievable contrast by up to one order of magnitude. Nevertheless, the predicted performance still meets the METIS contrast requirement (red star in Figure 9).

For the RAVC, including the before-mentioned effects, the 5- σ contrast for a bright ($L \leq 6$ mag) star at L band is estimated to be $\approx 2 \times 10^{-4}$ at $2 \lambda/D$ ($0.''046$), and $\approx 2 \times 10^{-5}$ at $5 \lambda/D$ ($0.''115$) after post-processing – see purple curve in Figure 9. The equivalent 5- σ contrast for the APP is estimated to be $\approx 2 \times 10^{-3}$ at $2 \lambda/D$, and $\approx 2 \times 10^{-5}$ at $5 \lambda/D$ after post-processing.

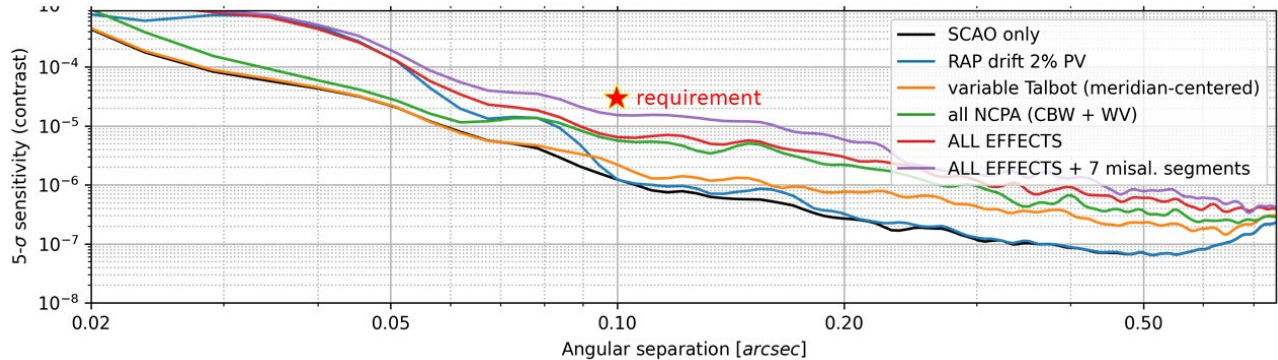


Figure 9 5- σ Contrast curves for METIS coronagraphy with the RAVC at $3.5 \mu\text{m}$ for a number of cases. The best case – no perturbations – is indicated by the black line; the purple line includes all effects considered. The METIS contrast requirement is shown as a red star at $5 \lambda/D$.

REFERENCES

- [1] Brandl, B. et al., “METIS: The Mid-infrared ELT Imager and Spectrograph”, *The Messenger*, vol. 182, p. 22-26 (2021)
- [2] Brandl, B. et al., “METIS: the thermal infrared instrument for the E-ELT”, *Proceedings of the SPIE*, Volume 8446, article id. 84461M, 13 pp. (2012)
- [3] Brandl, B. et al., “METIS: the mid-infrared E-ELT imager and spectrograph”, *Proceedings of the SPIE*, Volume 9147, id. 914721 18 pp. (2014)
- [4] Brandl, B. et al., “Status of the mid-infrared E-ELT imager and spectrograph METIS”, *Proceedings of the SPIE*, Volume 9908, id. 990820 15 pp. (2016)
- [5] Brandl, B. et al., “Proceedings of the SPIE, Volume 9908, id. 990820 15 pp. (2016)”, *Proceedings of the SPIE*, Volume 10702, id. 107021U 15 pp. (2018)
- [6] Pascucci, I., Herczeg, G., Carr, J. S., et al., *ApJ*, 779, 178 (2013)
- [7] Banzatti, A., Pontoppidan, K. M., Salyk, C., et al., *ApJ*, 834, 152 (2017)
- [8] Smith, R. L., Pontoppidan, K.M., Young, E.D., et al., *ApJ*, 701, 163 (2009)
- [9] Brown, J. M., Pontoppidan, K. M., van Dishoeck, E. F., et al., *ApJ*, 770, 94 (2013)
- [10] Teague, R., Bae, J., Bergin, E. A., et al., *ApJL*, 860, L12 (2018)
- [11] Pinte, C., Price, D. J., Ménard, F., et al., *ApJL*, 860, L13 (2018)
- [12] Andrews, S. M., Huang, J., Pérez, L. M., et al., *ApJL*, 869, L41 (2018)
- [13] Avenhaus, H., Quanz, S. P., Garufi, A., et al., *ApJ*, 863, 44 (2018)
- [14] Brogi, M., de Kok, R. J., Albrecht, S., et al., *ApJ*, 817, 106 (2016)
- [15] Birkby, J. L., de Kok, R. J., Brogi, M., et al., *AJ*, 153, 138 (2017)
- [16] Kasper, M., Arsenaault, R., Käufl, U., et al., *The Messenger*, 178, 5 (2019)
- [17] Quanz, S. P., Crossfield, I., Meyer, M. R., et al., *International Journal of Astrobiology*, 14, 279 (2015)
- [18] Anglada-Escudé, G., Amado, P. J., Barnes, J., et al., *nature*, 536, 437 (2016)
- [19] Zaalberg, D. et al., “Development of an aluminium mirror with a novel integrated flexure-based mount for cryogenic environment of METIS”, *Proceedings of the SPIE*, Volume 12188 [this meeting] (2022)

- [20] Maresca, M. et al., “Development and verification of the largest cryogenic mid IR aluminium concave mirror for METIS showing excellent wavefront performance”, Proceedings of the SPIE, Volume 12188 [this meeting] (2022)
- [21] Paalvast, S. et al., “Development and characterization of a 2D precision cryogenic chopper for METIS”, Proceedings of the SPIE, Volume 9151, id. 91510D 8 pp. (2014)
- [22] Correia, C.M., et al., “ELT METIS wavefront control strategy”, Proceedings of the SPIE, Volume 12185 [this meeting] (2022)
- [23] Bizenberger, P., et al., “METIS: Final design of the Imager sub-system”, Proceedings of the SPIE, Volume 12184 [this meeting] (2022)
- [24] Absil, O., et al., “Final design and expected performance of the METIS high-contrast imaging modes”, Proceedings of the SPIE, Volume 12184 [this meeting] (2022)
- [25] Agócs, T. et al., “Ge immersed grating manufacturing and optical verification for the METIS high-resolution spectrograph”, Proceedings of the SPIE, Volume 11451, id. 114511G 12 pp. (2020)
- [26] Bouzerand, E., et al., “The final design of the cryostat for ELT/METIS”, Proceedings of the SPIE, Volume 12184 [this meeting] (2022)
- [27] Amorim, A., et al., “A mass and vibration optimised solution for 6D precision heavy instrument alignment and its application to METIS”, Proceedings of the SPIE, Volume 12188 [this meeting] (2022)
- [28] Costa, R., et al., “The METIS warm support structure final design”, Proceedings of the SPIE, Volume 12184 [this meeting] (2022)
- [29] Filho, M., et al., “Manufacturing, Assembly and Integration of the WSS for METIS”, Proceedings of the SPIE, Volume 12187 [this meeting] (2022)
- [30] Kumar Sharma, T., et al., “Optical design, analysis, and performances of the infrared and visible channels of the Warm Calibration Unit in METIS/ELT”, Proceedings of the SPIE, Volume 12184 [this meeting] (2022)
- [31] Rutowska, M., et al., “Warm Calibration Unit of the mid-infrared ELT instrument METIS – overview and current status towards FDR”, Proceedings of the SPIE, Volume 12184 [this meeting] (2022)
- [32] Absil, O., et al., “Impact of water vapor seeing on mid-infrared high-contrast imaging at ELT scale”, Proceedings of the SPIE, Volume 12185 [this meeting] (2022)
- [33] Delacroix, C., et al., “The High-contrast End-to-End Performance Simulator (HEEPS)”, Proceedings of the SPIE, Volume 12187 [this meeting] (2022)
- [34] Shinde, M., et al., “Modeling the vortex center glow in the ELT/METIS vortex coronagraph”, Proceedings of the SPIE, Volume 12187 [this meeting] (2022)
- [35] Stuik, R., et al., “Preparing for system level AIV for METIS”, Proceedings of the SPIE, Volume 12184 [this meeting] (2022)
- [36] Sabha, N., et al., “The spectroscopic pipeline design of the ELT METIS”, Proceedings of the SPIE, Volume 12189 [this meeting] (2022)